Toxicology Research

PAPER

View Article Online
View Journal | View Issue

Cite this: *Toxicol. Res.*, 2016, **5**, 303

Evaluation of the intracellular uptake and cytotoxicity effect of TiO_2 nanostructures for various human oral and lung cells under dark conditions

Chieh-Wei Chen,[a] Jing-Hong Huang,[a] Tsung-Ching Lai,[b] Yi-Hua Jan,[b] Michael Hsiao,*[b] Chung-Hsuan Chen,[b] Yeu-Kuang Hwu[c] and Ru-Shi Liu*[a,b,d]

Received 31st August 2015,
Accepted 17th November 2015

DOI: 10.1039/c5tx00312a

www.rsc.org/toxicology

Titanium dioxide (TiO_2) nanomaterials (NMs) have been widely used to develop commercial products such as sunscreen cosmetics because of their unique optical properties to provide complete protection from ultraviolet (UV) light. The most dangerous type of UV radiation is UVA, which comprises nearly 97% of the UV radiation that reaches the Earth. This type of radiation is also the major cause of skin damage. As the most beneficial content of sunscreen cosmetics, TiO_2 NMs exhibit immense capability to protect the human skin from UVA exposure through their scattering and reflecting physical properties. Therefore, investigating the factors involved in using TiO_2 NMs in cosmetics is necessary. In this study, various human oral and lung cell lines were selected to evaluate the cytotoxicity of treatment using different sizes and shapes of TiO_2 NMs, including spheres (AFDC and AFDC300) and rods (M212 and cNRs). The morphology, size, and crystalline phase of the selected TiO_2 NMs were studied to characterize each physical property. Based on cell viability and endocytic behavior results, treatment with all the selected TiO_2 NMs were nearly non-toxic to the oral cell lines. However, high cytotoxicity was obviously observed in lung cells with M212 and AFDC treatments at 50 μg mL^{-1}, which was larger by approximately 20% than with ADC300 and cNRs treatments because the smaller the TiO_2 NMs, the larger their specific surface area. This condition resulted in the progress of apoptosis from the considerable aggregation of TiO_2 NMs in the cytoplasm. Moreover, compared with those of TiO_2 NMs with a similar structure (*e.g.*, cNRs) and size (*e.g.*, M212), the cellular uptake of AFDC was evidently low, which resulted in the approximated non-toxicity. Moreover, the similar sizes and different shapes of AFDC and cNRs were considered to treat lung cells to investigate further the influence of morphology on the cell cycle and the apoptosis effect. Consequently, AFDC and cNRs could inhibit the growth of lung cells and allow a considerable proportion of the cells to remain in the G1/G0 phase. Furthermore, a high-dose treatment would directly induce the apoptosis pathway, whereas a low-dose treatment might decrease cell regeneration.

Introduction

Ultraviolet (UV) radiation occupies the wavelength range of 100–400 nm in the solar spectrum and is divided into mainly three parts, namely, UVC (100–280 nm), UVB (280–315 nm), and UVA (315–400 nm). The highest UVC energy in UV radiation has the lowest potential risk because a considerable proportion of UVC is significantly reduced by the protective layer of ozone in the atmosphere. However, UVA and UVB can still penetrate into the surface of the Earth and pose a direct threat to human health, particularly the skin.[1] After passing through the atmospheric layer, UVA occupies 95% of the residual component that has a major influence on human skin compared with only 5% UVB. Therefore, sunscreen cosmetics, which can be used to reflect or scatter UVA to prevent direct damage to the skin, have been developed. Nanomaterials (NMs) have been investigated extensively by researchers from various fields to develop commercial cosmetics with sunscreen function because many physical and chemical properties of these NMs are considerably modified by the size effect.[2–6] Among these materials, titanium dioxide (TiO_2) NMs have been developed into excellent additives in sunscreen cosmetics because they can be used as a UV absorbent with a 3.2 eV band gap and can support physical effects, such as scattering and reflection, to

[a]*Department of Chemistry, National Taiwan University, Taipei 106, Taiwan. E-mail: rsliu@ntu.edu.tw*
[b]*Genomics Research Center, Academia Sinica, Taipei 115, Taiwan. E-mail: mhsiao@gate.sinica.edu.tw*
[c]*Institute of Physics, Academia Sinica, Taipei 115, Taiwan*
[d]*Department of Mechanical Engineering and Graduate Institute of Manufacturing Technology, National Taipei University of Technology, Taipei 106, Taiwan*

decrease UVA radiation exposure.[7–10] Therefore, adding nanoparticles to sunscreen cosmetics is a powerful means to protect the skin from exposure to UVA radiation through chemical absorption and physical interaction. The previous literature has determined that under UV light exposure, TiO_2 NMs will generate reactive oxygen species (ROS), such as superoxide radical anions ($O^{2-\bullet}$), hydrogen peroxide (H_2O_2), and $^{\bullet}OH$ radicals, that can potentially damage intracellular DNA and membranes.[11–17] In addition, many other uncertain risk factors should also be considered, such as the accumulation of nanoparticles in the human body and their direct contact with inner cells. TiO_2 NMs passes through two routes to invade human organs directly: (1) exposure of oral cells through ingestion and (2) exposure of lung cells through respiration. Although no UV radiation may get inside the body to induce the photocatalysis of TiO_2 NMs, the nature of TiO_2 NMs may promote unknown effects inside the body under dark conditions. Therefore, assessing cellular response to different sizes and concentrations of TiO_2 NMs with respect to cytotoxicity is important to evaluate the potential risk of further applications of these materials. Moreover, the cytotoxicity effects of different types of TiO_2 NMs were investigated under dark conditions because we aimed to inhibit their capability to produce ROS intracellularly. Notably, numerous researchers have attempted to investigate the toxicity of TiO_2 NMs in the environment or in oceans because some TiO_2 NMs are randomly released into the natural environment, including the soil, rivers, and marine habitats, and thus, will indirectly accumulate in plants and animals.[18] Rocheleau *et al.*[19] studied the toxicity of TiO_2 materials in the soil nematode *Caenorhabditis elegans* (*C. elegans*) in bulk and nanoscales in anatase and rutile crystalline phases. Interestingly, these researchers determined that the size of TiO_2 materials did not obviously influence cytotoxicity in *C. elegans*; however, different crystalline phases passed through various metabolic pathways. Tong *et al.*[20] focused on exploring different treatment methods for bacteria with either a single component or a mixture of various nanomaterials, such as ZnO and TiO_2. Based on their results, the cytotoxicity of nanomaterials was more complex in mixed systems because a considerable variable would be generated from the interaction among nanomaterials. Numerous studies have also investigated the toxicity effects of various properties of TiO_2 materials. In our study, several treatment condition factors and various physical properties of TiO_2 NMs were selected, including exposure concentration, size, crystalline phase, shape, and surface area, among others.[21–24] To our knowledge, studies on the toxicity effect of TiO_2 NMs should first consider irradiated light because semiconductor TiO_2 NMs exhibit an immense potential to generate ROS, which will induce considerable damage to tissues and cells. The size, shape, and surface area of TiO_2 NMs are key issues that influence cellular interaction and dose dependence, as concluded by several studies with different cases or targets (*e.g.*, bacteria, zebrafish, mice). However, most of these studies only verified one or two factors simultaneously. Based on these studies, we aimed to investigate in detail the cytotoxicity effect of treatment with TiO_2 NMs on various human cell lines given that TiO_2 NMs are applied extensively and intimately in daily life, but only a few studies had addressed this issue. The physical characteristics of TiO_2 NMs are also reported in this paper.

In this study, the cytotoxicity effects of TiO_2 NMs were investigated in terms of three main points: morphology, size, and cell line type. Human oral and lung cells, including Smulow–Glickman (S–G) gingival epithelial cells, oral mucosa fibroblasts (OMFs), normal human bronchial epithelial cells (BEAS), and lung fibroblasts (WI-38) were exposed to TiO_2 NMs with different structures, such as AFDC, AFDC300, M212, and cNRs (cNRs were extracted directly from commercial cosmetics) and varying sizes, namely, 142 ± 22.7, 214 ± 46.1, 28 ± 8.4/10 ± 1.4 and 117 ± 12.5/39 ± 7.8 nm (length/width), respectively. These cell types were selected to study the cytotoxicity effect because they were directly exposed to nanoparticles through respiration and ingestion. We also intended to identify the direct reasons or the mechanism of TiO_2 NM cytotoxicity in these human cell types. The intracellular uptake of various TiO_2 NMs was investigated *via* transmission electron microscopy (TEM) to determine the localization of TiO_2 NMs inside the cells because these materials did not emit fluorescence or magnetic properties for magnetic resonance imaging. To study the cellular response of TiO_2 NM-treated cells and identify the mechanism of cytotoxicity, an apoptosis assay and cell cycle analysis were performed.

Results and discussion

To characterize the size and shape of individual TiO_2 NMs, TEM was performed to determine the difference between each group of TiO_2 NMs, namely, M212, AFDC, AFDC300, and cNRs. As shown in Fig. 1(A)–(C), M212 has a rod shape with a length of 28 ± 8.4 nm and a width of 10 ± 1.4 nm, whereas AFDC and AFDC300 are spherical with a diameter of 142 ± 22.7 nm and 214 ± 46.1 nm, respectively. As shown in Fig. 1 (D), cNRs have a spindle shape with a length of 117 ± 12.5 nm and a width of 39 ± 7.8 nm. Notably, the TEM images of the NMs had a low contrast compared with the background because of poor crystallization. Calculating the precise size of each TiO_2 NM was difficult. The crystalline phase of each TiO_2 NM was confirmed by powder X-ray diffraction (XRD) analysis, as shown in Fig. 2. The XRD patterns of M212 and cNRs matched well with the rutile standard (JCPDS no: 21-1276). Meanwhile, AFDC and AFDC300 matched well with the anatase crystalline phase based on the anatase standard (JCPDS no: 21-1272). The anatase crystalline phase of TiO_2 NMs exhibited better photocatalytic capability than the rutile crystalline phase because of the relatively large band gap in this phase for inducing free radical reactions under sunlight excitation. Based on this feature, the rutile crystalline phase of TiO_2 NMs, such as cNRs and M212, has always been a major option in sunscreen cosmetic technology.[25,26] Therefore, considering the inhibition of ROS production, all cytotoxicity studies on the two crystal phases of TiO_2 NMs were performed

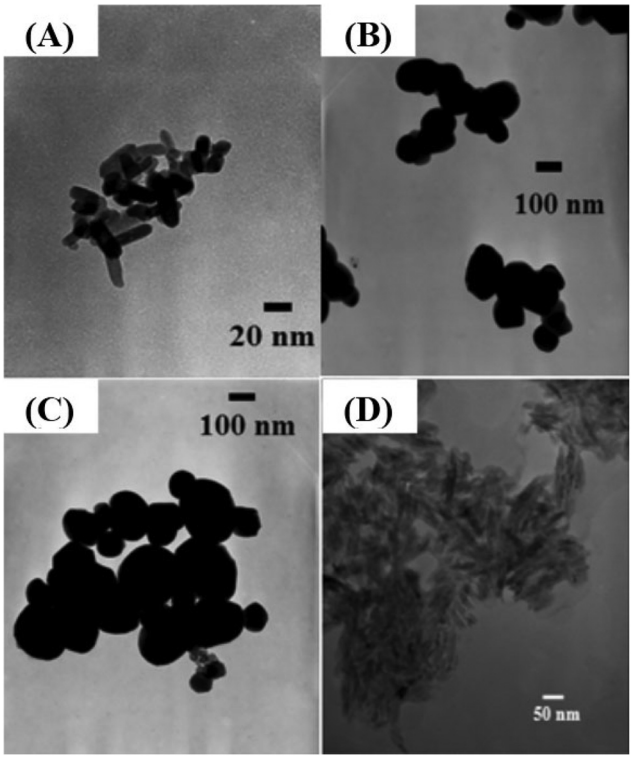

Fig. 1 TEM images of the TiO_2 NMs: (A) M212, (B) AFDC, (C) AFDC300, and (D) cNRs.

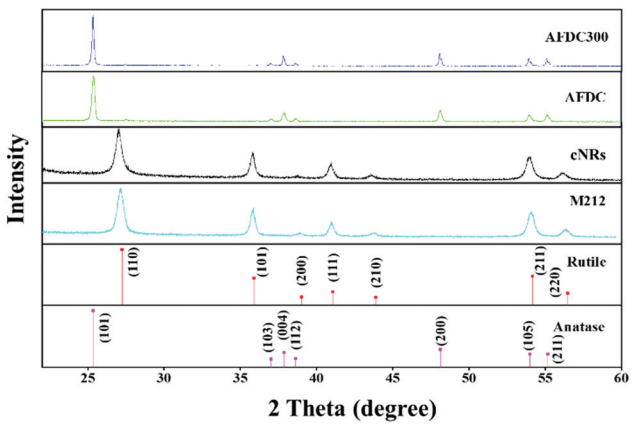

Fig. 2 XRD patterns of M212, AFDC, AFDC300, and cNRs. Standard patterns of the rutile and anatase crystalline phases of TiO_2.

under dark conditions to ignore factors such as photocatalysis. To study the effects of the shape and size of TiO_2 NMs on oral and lung cells, all the TiO_2 NMs were incubated with various oral and lung cells to study cytotoxicity further. The interaction of cellular endocytosis was investigated before the cell viability test was performed to confirm that TiO_2 NMs entered the cells.

TEM was performed to identify intracellular location and evaluate the cellular uptake of various sizes and shapes of TiO_2 NMs. Through TEM, the localization of each TiO_2 NM in different oral and lung cells, namely, S–G, OMF, BEAS, and WI-38, was identified. All the TEM images show the cross section of the cells to identify the subcellular localization of the TiO_2 NMs within the cells. As shown in Fig. 3, each TiO_2 NM was internalized by cells and aggregated into the cytoplasm instead of the nucleus. Notably, the amount of cellular uptake did not considerably differ among each type of cells. We focused on the various sizes and structures of TiO_2 NMs that could affect intracellular interaction. M212, AFDC, and AFDC300 exhibited significant aggregation in the cytoplasm of all the studied oral and lung cells after treatment for 72 h. Meanwhile, the cellular uptake of cNRs was lower probably because of its spindle shape with approximately 120/40 nm, which caused poor interaction among the cells. Based on the results, M212, which was smaller and rod shaped at only 30/10 nm, induced the highest aggregation rate because of its high surface energy and specific surface area. The high uptake observed in the cases of AFDC and AFDC300 indicated that cell membranes could easily interact in a spherical shape and be further internalized into the cytoplasm. Meanwhile, when cNRs and AFDC, which had similar sizes, were compared, the results demonstrated that the long spindle shape of cNRs interfered with endocytosis.[27,28] Regardless of the rod or spherical structure of TiO_2 NMs or a relatively large size ranging from 30 nm to 250 nm, uptake into the cytoplasm was confirmed to be achieved through endocytosis. Moreover, the size of TiO_2 NMs was a key factor in the aggregation of cells inside the cytoplasm because of the large specific surface area for a small size. Therefore, after the exposure of oral and lung cells, TiO_2 NMs were determined to pose uncertain risks to cell life through direct contact and endocytosis. To evaluate the cytotoxicity of individual TiO_2 NMs incubated with the four cell lines, an MTS assay was performed to investigate the relative influence of cellular uptake on cell viability.

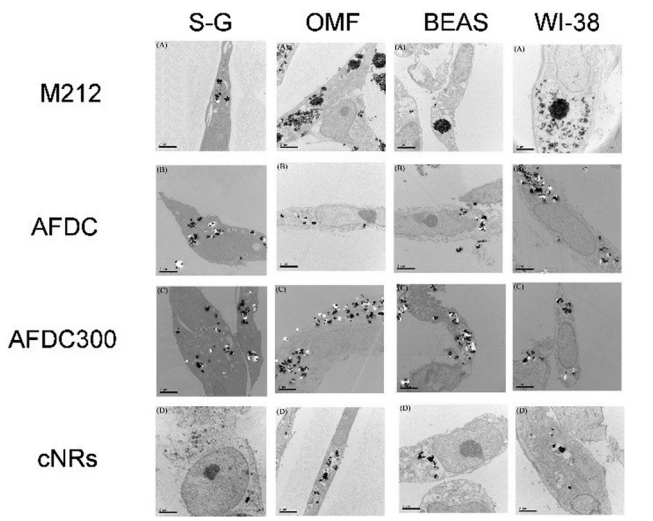

Fig. 3 TEM images of the S–G, OMF, BEAS-2B, and WI-38 cell lines after treatment with various sizes of TiO_2 NMs (M212, AFDC, AFDC300, and cNRs).

Fig. 4(A)–(D) show the viability of the oral and lung cells after being incubated with 0, 12, 50, 200, and 800 μg mL^{-1} TiO_2 NMs (the latter four correspond to M212, AFDC, AFDC300, and cNRs, respectively) for 72 h. The cell viability trend decreased with increasing concentrations of TiO_2 NMs for each cell line because the high TiO_2 concentration interfered with cell viability through considerable TiO_2 uptake. However, both types of oral cells exhibited a viability of nearly over 80%, which resulted in the estimated lack of influence of all the studied TiO_2 NMs. Based on these results, the discussion would first focus on the variation in cell viability of lung cells. Among these, AFDC and M212 presented relatively high toxicities in S–G and OMF because their considerable internalization and aggregation in the cytoplasm (based on the TEM images), affected the normal growth environment of the cells.[17] Moreover, the morphology factor was also reflected on the difference in cell viability. Meanwhile, the comparison of NMs with similar sizes, such as AFDC and cNRs, indicated that cells treated with cNRs displayed a relatively high cell viability than those treated with AFDC because the progress of endocytosis preferred materials with a spherical shape, which could easily and effectively interact with cell membranes.[29] Moreover, based on the literature, the crystalline phase of materials is an important factor that affects cytotoxicity in cells because each crystalline phase can reveal certain differences in their surface area.[30] For TiO_2 NMs, the average surface area was ~200 m^2 g^{-1} and 2.5 for the anatase and rutile crystalline phases, respectively, which indicated that TiO_2 NMs with an anatase crystalline phase interacted approximately 80 times with the cell membrane.[31,32] This result could also be indicated by AFDC, which had an anatase crystalline phase, exhibiting higher toxicity than cNRs even though they were similar in size. For the oral cell lines, S–G cells had higher viability upon exposure to various concentrations of TiO_2 NMs than OMF cells because of the tolerance of different cells. The unknown risk of treating oral cells with high concentrations of TiO_2 NMs indicated that lung cells, such as BEAS and WI-38, were more sensitive than oral cells to TiO_2 NMs in a concentration-dependent manner. Compared with other cell types such as keratinocytes and fibroblasts, different trends were observed for lung and oral cells. This finding suggested that various types of cells exhibited different endocytosis mechanisms and tolerance levels to TiO_2 NMs depending on their capabilities. Consequently, other factors or mechanisms that might cause differences in the cytotoxicity results between AFDC and cNRs would be identified and further investigated later. Lung cells exhibited the most sensitive reaction to TiO_2 NMs because the cytotoxicity presented a significant difference. In particular, the damage caused by TiO_2 NMs in BEAS cells was more serious than those in WI-38 cells. Based on the cytotoxicity results, the BEAS cell line was selected for further apoptosis and cell cycle analysis because of its low viability.

The flow cytometry analysis of an apoptotic cell is shown in Fig. 5. Annexin-V was used to detect the early stage of apoptosis, and a DNA staining dye (7-AAD) was used to determine the integrity of the membrane structure during the latter stage of apoptosis. The signal of the *x* axial (PE-A) resulted from the staining of annexin positive membrane cells. The intensity of

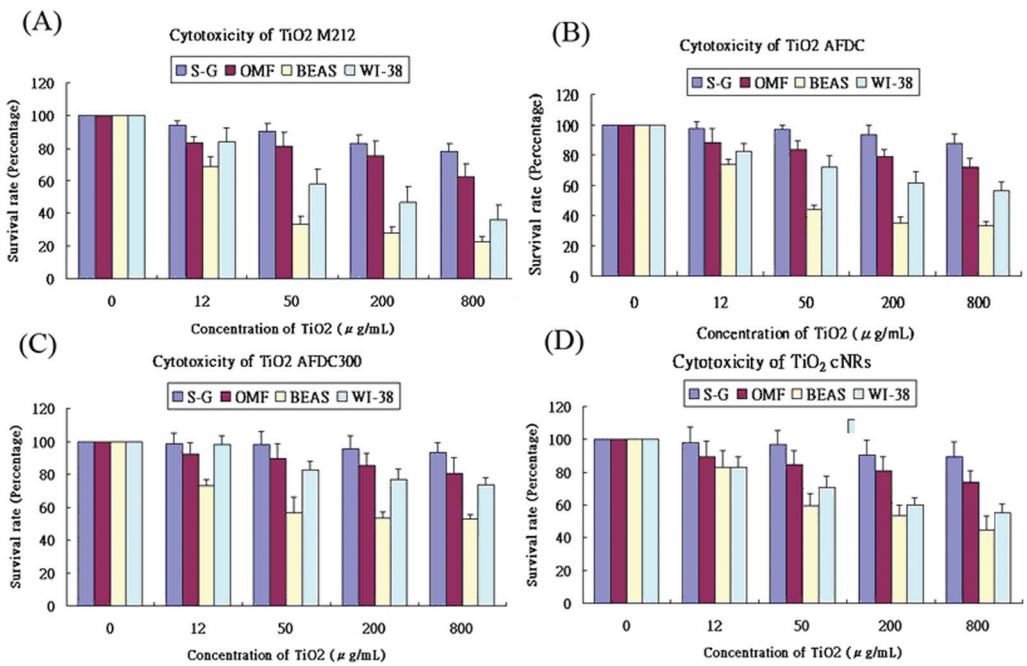

Fig. 4 Cytotoxicity of TiO_2 NMs. Cytotoxicity effects on (A) M212, (B) AFDC, (C) AFDC300, and (D) cNRs. S–G, OMF, BEAS, and WI-38 treated with different doses (0, 12, 50, 200, and 800 μg mL^{-1}) of TiO_2 NMs for 24 h. Cell viability was assessed *via* the MTS assay. Data were expressed as the percentage of viability related to an untreated control. Viability values were calculated as the mean + SD of eight experiments.

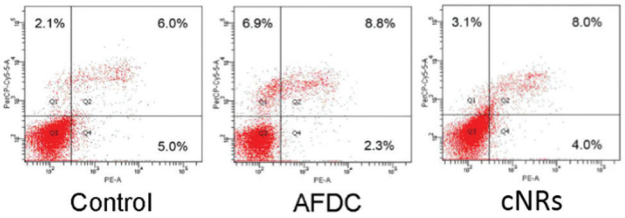

Fig. 5 Apoptosis analysis of BEAS-2B cells. Cells were treated with different types of TiO_2 NMs (AFDC and cNRs) at a concentration of 12 μg mL^{-1} for 72 h. After annexin-V/7-AAD double staining, the percentage of apoptotic cells was analyzed *via* flow cytometry.

the *y* axial (PerCP-Cy5-5-A) was obtained from the signal of the staining DNA in the broken membrane cells. AFDC and cNRs were chosen for the apoptosis analysis because of their different shapes and similar sizes of approximately 150 nm. After treatment with 100 μg mL^{-1} TiO_2 NMs for 72 h, the apoptosis of BEAS cells was determined with annexin-V–phycoerythrin (PE) to represent the distortion of membrane asymmetry. The proportions of early apoptotic cells treated with AFDC and cNRs decreased to 2.3% and 4.0% compared with the 5.0% in the control experiment. However, the proportions of late apoptotic step and necrotic cells increased to 8.8% and 8.0% compared with the 6.0% in the control experiment. These findings indicated that TiO_2 NMs induced a small amount of BEAS cells during the early step of apoptosis until its late step because of the decreasing proportion of early apoptotic cells. Although the increasing proportion of the late apoptotic step cells compared with that in the control experiment displayed a relative incompleteness of cell membrane increase, the difference value of approximately 2% between them was too small to distinguish cell apoptosis between the control experiment and the TiO_2-treated cells clearly. Hence, the late apoptotic step was not mainly responsible for the decrease in cell viability and could not be compared with the cytotoxicity analysis, which revealed an estimated 20% difference between the viability of the AFDC- and cNRs-treated cells as well as a considerable decrease in cell viability compared with that in the control. The result suggested that the membranes of BEAS cells retained their completeness or were slightly defeated compared with the control experiment; hence, TiO_2 NMs could not cause the immediate death of BEAS cells. Further investigations were conducted to perform cell cycle analysis and understand the influence of TiO_2 NMs.

A cell cycle involves a series of regular steps, that is, the cells grow and then divide into two daughter cells. The cell cycle can be divided into the cell growth stage and mitosis. The former can be generally classified into three phases: G1, S, and G2. In the first phase (G1), cells are prepared to actively replicate the substances, as well as some cytoplasmic organelle composition, for the next step. During the S phase, DNA is replicated, and cells with double genetic materials are prepared for mitosis during the G2 phase. During mitosis, cells undergo the chromosome segregation and cytokinesis stages. In addition, a G0 phase, which indicates that cells are terminating the division process, also exists. The variation in cell cycle was analyzed *via* a flow cytometry technology shown in Fig. 6. The G1/G0 phase represents the interphase during cell growth, which is from the end of the previous mitosis phase (M) until the beginning of the DNA synthesis/quiescent state. During the G1/G0 phase, the intensity of PE-A indicates the DNA content of the cells. As DNA replication in the synthesis phase (S) is completed, two pairs of chromosomes are formed and move toward the G2 phase, which causes the intensity of PE-A to double. In the control experiment, the proportion of BEAS cells in the G1/G0 phase decreased to 45.9% (after 36 h of incubation) and 49.2% (after 72 h of incubation) from 51.4% in the control experiment. For the G2/M phase, the proportion decreased to 25.1% (after 36 h of incubation) and 26.1% (after 72 h of incubation) from the original 28.2%. These findings showed that the cell cycle was sufficiently stable to precede reproduction within 72 h without any significant change. However, 26.1% of the cell proportion in the G2 phase decreased to 6.7% and 10.4% after treatment with AFDC and cNRs, respectively, for 72 h (the 25.1% cell proportion in the G2 phase decreased to 6.6% and 11.0% after treatment with AFDC and cNRs, respectively, for 36 h). By contrast, the 49.2% cell proportion in the G1 phase increased to 66.8% and 63.2% after treatment with AFDC and cNRs, respectively, for 72 h (the 45.9% cell proportion in the G1 phase increased to 65.2% and 59.5% after treatment with AFDC and cNRs, respectively, for 36 h). The results could be concluded as either the inhibition or improvement of BEAS cell growth, both of which decreased the proportion during the G2 phase/M phase.[33–35] Based on the cytotoxicity results (Fig. 4), cell viability decreased relatively compared with the amount of cells in the control experiment. Hence, cell reproduction was restrained under the treatment of 100 μg mL^{-1} TiO_2 NMs. Consequently, the proportion of cells in the G2/M phase decreased with increasing cell proportion in G1/G0. BEAS cells might get injured after TiO_2 uptake by endocytosis and aggregation

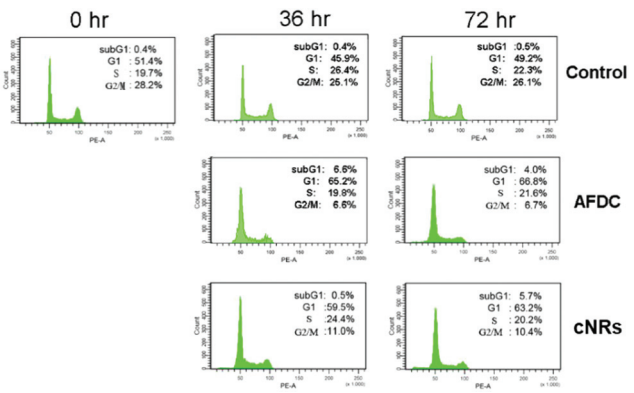

Fig. 6 Cell cycle analysis of BEAS cells treated with TiO_2 NMs (AFDC and cNRs) at a concentration of 12 μg mL^{-1} for 36 h and 72 h. After staining with propidium iodide, cell cycle distribution was analyzed *via* flow cytometry.

within cells to change the protein action against growth in these cells.

As shown in Fig. 7(A), as the concentration of AFDC increased by up to 800 μg mL^{-1} after incubation for 36 h and 72 h, an apparent increase to 25.2% (36 h) and 49.8% (72 h) in the subG1 phase was observed compared with the control experiment. This finding indicated that the amount of cells with broken DNA increased with increasing the TiO_2 content. In one part of G2/M, a significant decrease from 28.8% to 13.9% (36 h) and 2.3% (72 h) indicated cessation of regeneration. The high concentration of TiO_2 NMs (800 μg mL^{-1}) treatment induced serious apoptosis of BEAS-2B after 72 h of incubation. However, in the comparison between BEAS-2B treated with 12 μg mL^{-1} and 800 μg mL^{-1} TiO_2, only the BEAS-2B cells stopped growing further without an apparent cell apoptosis at 12 μg mL^{-1}. The different consequences between these two cases resulted from the concentration effect. Hence, exposure to high concentrations of TiO_2 NMs was toxic to BEAS-2B cells. After the BEAS cells were treated with AFDC for 72 h, the obvious decrease from 31.4% (control) to 2.3% during G2/M demonstrated the inhibition of cell proliferation because of the considerable amount of apoptotic cells. Thus, exposure to high concentrations of TiO_2 NMs may cause severe damage to lung epithelial cells, which is comparable with the cytotoxicity results in high concentrations. The results of the cytotoxicity assay could be attributed to different causes as follows. In the low-concentration treatment, the cell cycle of BEAS-2B cells was terminated during the G1/G0 phase without apparent cell death. This result indicated that decreasing regeneration led to a decrease in cell numbers compared with that in the control. In the high-concentration treatment, the dramatic decrease in cell viability was contributed by apoptotic cell death.

To determine the apoptosis mechanism of BEAS-2B cells induced by high concentrations of AFDC, Western blot analysis was performed to identify the route of caspase activation. Fig. 7(B) shows that caspase-8 has been activated at 48 h, whereas no activation of caspase-9 has been detected. This figure also shows that caspase-3, which is a direct substrate of caspase-8, has been activated at 72 h. Finally, the cleavage of poly(ADP-ribose)polymerase (PARP) at 72 h indicated the apoptosis marker. To confirm that AFDC induced apoptosis, caspase-3/7 activity test was conducted to identify performance. In Fig. 7(C), the signal increased with time-dependent treatment and the change was not observed after reaction with the caspase-8 inhibitor. Therefore, treating BEAS-2B with a high-concentration of AFDC resulted in an apoptosis pathway through the expression of caspase-8, which corresponded to caspase-3/7 activation.

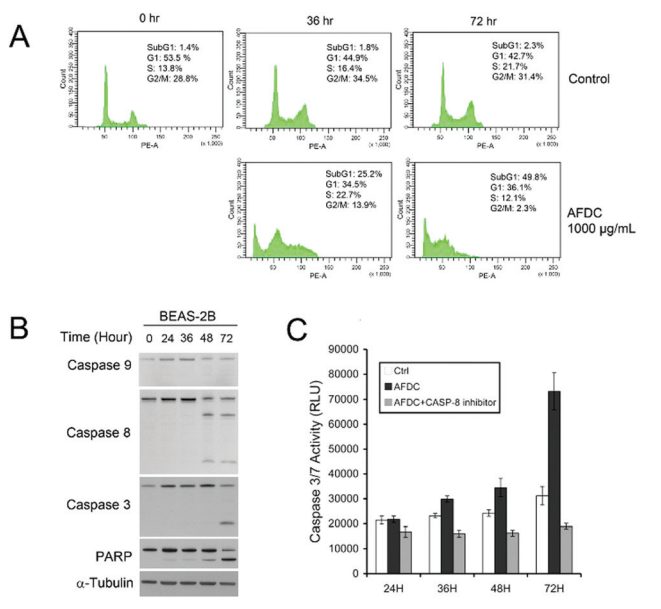

Fig. 7 (A) Cell cycle analysis of BEAS cells treated with a high concentration of AFDC (800 μg mL^{-1}) for 36 h and 72 h. (B) Western blot analysis of caspase-9, caspase-8, caspase-3 and PARP expression in BEAS-2B cells treated with AFDC (1000 μg mL^{-1}). (C) Caspase-3/7 activity of BEAS cells treated with a high concentration of AFDC (1000 μg mL^{-1}) with or without the caspase-8 inhibitor for 24, 36, 48, and 72 h.

Conclusion

The physical properties of each TiO_2 NM, including commercial TiO_2 NMs (M212, AFDC, and AFDC300) and cNRs extracted from commercial sunscreen cosmetics, were all clearly verified in terms of size, morphology, and crystalline phase. The cellular endocytosis behavior in TiO_2 NMs confirmed their relationship with various sizes (minor) and morphologies (major). That is, a small and sphere-shaped TiO_2 NM would uptake more than a large and rod-shaped TiO_2 NM. TiO_2 NMs were aggregated in the cytoplasm. The cytotoxicity assay exhibited the high toxicity of M212 with a small particle size, which aggregated seriously in the cytoplasm. After treatment with AFDC and cNRs at a concentration of 100 μg mL^{-1}, the apoptosis of BEAS cells exhibited only a 2% difference from the control experiment, which did not obviously influence the late stage of apoptosis to induce cell death; hence, the death of cells could not be concluded. The result suggested that TiO_2 NMs could not cause immediate cell death because of the unchanged completeness of the cell membrane. Cell cycle arrest was observed under exposure to low concentrations of TiO_2, whereas high concentrations of TiO_2 treatment could cause cell cytotoxicity and apoptosis. BEAS cells obviously died because of the appearance of a signal in the sub-G1 section. In summary, the size effect induced the easy aggregation of small particles. The shape factor hindered TiO_2 uptake. TiO_2 concentration led to different degrees of cell cycle arrest between 100 μg mL^{-1} and 1000 μg mL^{-1} in a concentration-dependent manner. High concentrations of AFDC (1000 μg mL^{-1}) could induce apoptosis of BEAS-2B cells through caspase-8 mediated caspase-3/7 activation. In this study, we aimed to evaluate the cytotoxicity effect of TiO_2 NMs under dark conditions and determined that the major toxicity risk was first dependent on the cell line type and highly related to the size and morphology

of TiO_2 NMs because these factors affected intracellular uptake and cell growth behavior, respectively.

Experimental

Reagents and materials

The nanoparticle-containing sunscreen cosmetic was purchased from a well-known company. Commercially available TiO_2 NMs (M212, AFDC and AFDC300) were purchased from Top Rhyme International Company. Acetone (>99.5%, Sigma-Aldrich), absolute ethanol (99%, Riedel-de Haen) and *n*-hexane (99%, Riedel-de Haen) were used as purchased without further purification.

Extraction of TiO_2 NMs

First, 1.5 g sunscreen cosmetic was dissolved into a 50 mL mixture solvent, which contained absolute ethanol, acetone, and *n*-hexane. This procedure was followed by ultrasonication for 20 min. Then, the product of cNRs (white powder) was obtained by centrifugation at 9000 rpm for 20 min. After removing the supernatant, the products were collected and stored in a 50 mL tube, and then dried in an oven at 70 °C for 30 min. To purify the products, the preceding procedures were repeated several times until organic species were completely removed from the samples. Finally, a pure white powder (cNRs) was obtained for further analysis.

Cell culture

Four cell lines were used in this study, namely, WI-38, BEAS, OMFs, and S–G gingival epithelial cells. WI-38 cells were cultured in minimum essential medium (Grand Island, NY, USA). BEAS cells were maintained in bronchial epithelial cell basal medium (Lonza, Walkersville, MD, USA) that contained bronchial epithelial growth medium (SingleQuots, Lonza, Walkersville, MD, USA). OMF and S–G cells were cultured in Dulbecco modified Eagle's medium (Gibco, Grand Island, NY, USA) supplemented with 10% (v/v) fetal bovine serum (Hyclone, CA, USA). All media were supplemented with 100 units per mL penicillin (Gibco, Grand Island, NY, USA) and 100 mg mL^{-1} streptomycin (Gibco, Grand Island, NY, USA).

Intracellular uptake analysis

Each cell line was used in this study. Exponentially growing cells (1×10^6 cells) were seeded in a 10 cm petri dish and incubated overnight at 37 °C under a 5% CO_2 atmosphere. The medium was replaced with a fresh one that contained 100 μg mL^{-1} TiO_2 NMs and incubated for another 72 h. After treatment with TiO_2 NMs, the cells were washed thrice with a serum-free culture medium. Subsequently, cells were fixed in 2% glutaraldehyde for 1 h and rinsed thrice for 5 min with a serum-free culture medium. Thereafter, sections were fixed in 0.25% aqueous osmium tetroxide and rinsed thrice with distilled water under a fume hood. Samples were dehydrated in ethanol (100%), infiltrated with 30% quetol in acetone for 1 h, further infiltrated with 60% quetol in ethanol for 1 h, and treated with pure quetol for 4 h thereafter. Sections were polymerized at 65 °C for 24–36 h. Ultra-thin sections were mounted on grids, contrasted for 10 min in 4% aqueous uranyl acetate, and rinsed in water. Contrast was enhanced by placing the samples in Reynolds' lead citrate for 2 min and then rinsing them with water. Samples were cut into 0.5 mm monitor sections, stained with toluidine blue, and immersed in immersion oil for TEM.

Cell viability analysis

The cytotoxicity effect of TiO_2 NMs on cell viability was determined *via* the MTS (3-(4,5-dimethylthiazol-2-yl)-5-(3-carboxymethoxy-phenyl)-2-(4-sulfonyl)-2*H*-tetrazolium) assay. Briefly, cells (2000 cells per 100 μL) were seeded onto 96-well plates and incubated overnight at 37 °C under a 5% CO_2 atmosphere. The medium in the wells was replaced with a fresh one that contained TiO_2 nanoparticles (0, 12, 50, 200, and 800 μg mL^{-1}) and incubated for another 72 h. After 72 h of incubation with various concentrations of TiO_2 NMs, 20 μL MTS reagent was added into each well of the 96-well plate. Cells were incubated for up to 3 additional hours at 37 °C. The absorbance in each well was analyzed on a plate reader using an exciting source with a 490 nm wavelength to determine cell viability.

Flow cytometric analysis of cell cycle

Cell cycle distribution was quantified by flow cytometry. BEAS cells were treated for 36 h and 72 h with TiO_2 NMs (AFDC and cNRs) at 100 μg mL^{-1} concentration. At the end of incubation, the cells were collected and resuspended in 70% ice-cold methanol. After fixation at −20 °C overnight, the cells were treated with 1 mg mL^{-1} RNase for 30 min at room temperature. Propidium iodide was added into the solution at a final concentration of 50 mg mL^{-1}. The cell cycle was analyzed *via* FACScanto flow cytometry, and data were analyzed using CellQuest software.

Flow cytometric analysis of apoptosis

Apoptotic cells were identified using FITC Annexin-V Apoptosis Detection Kit II (BD Pharmingen, USA). A cell death marker, 7-aminoactinomycin D (7-AAD), was also used according to the protocol of the manufacturer. Oral and lung cells (2×10^5 cells) were exposed to TiO_2 NMs (100 μg mL^{-1}) for 72 h, detached by trypsin-EDTA, washed with phosphate buffered solution (PBS), and stained with 5 μL annexin-V and 5 μL 7-AAD for 15 min in the dark. Apoptosis was analyzed *via* FACScanto flow cytometry, and the results were investigated using CellQuest software.

Caspase-3/7 activity assay

The activity of caspase-3/7 was quantified using Caspase-Glo 3/7 assay (Promega Corporation, Fitchburg, WI, USA). Cells were seeded at a density of 10^3 cells per well in a 100 μL medium. After 24 h of incubation, the culture media were replaced with 100 μL media that contained 1000 μg mL^{-1} AFDC TiO_2 TMs. At different incubation periods (24, 36, 48 and 72 h), caspase-3/7

activity was determined by adding 100 μL Cell Titer Glo reagent to each well and then incubating at room temperature for 30 min in the dark. Luminescence was detected and recorded using a luminometer according to the protocol of the manufacturer. Caspase-3/7 activity was calculated as a percentage compared with the untreated control at different time points.

Western blot analysis

Equal quantities of protein (20 μg) were separated by SDS-PAGE and transferred onto nitrocellulose membranes (Amersham Bioscience, Buckinghamshire, UK) using a Bio-Rad wet transfer system. After blocking with 5% non-fat dried milk in PBS + Tween 20 buffer for 1 h at room temperature the membranes were incubated with PARP antibody, cleaved PARP antibody, caspase-3, and α-tubulin antibody for 1 h at room temperature, followed by incubation with horseradish peroxidase-conjugated secondary antibody for 1 h at room temperature. Proteins were visualized *via* enhanced chemiluminescence.

Author contributions

The manuscript was written through the contributions of all the authors. All the authors have approved the final version of the manuscript.

Acknowledgements

The authors would like to thank the Department of Health, Executive Yuan under Contract no. DOH97-TD-D-113-97002, the Ministry of Science and Technology of Taiwan (Contract no. MOST 104-2113-M-002-012-MY3), and Academia Sinica (Contract no. AS-103-TP-A06) for financially supporting this research. We are also grateful to Ms C. Y. Chien of the Precious Instrument Center (National Taiwan University) for her assistance in the TEM experiments.

Notes and references

1 A. P. Popov, A. V. Priezzhev, J. Lademann and R. Myllylä, *J. Appl. Phys.*, 2009, **105**, 102035.
2 A. P. Popov, S. Haag, M. Meinke, J. Lademann, A. V. Priezzhev and R. Myllylä, *J. Biomed. Opt.*, 2009, **14**, 021011.
3 J. Lademann, H. J. Weigmann, C. Rickmeyer, H. Barthelmes, H. Schaefer, G. Mueller and W. Sterry, *Skin Pharmacol. Physiol.*, 1999, **12**, 247–256.
4 A. P. Popov, J. Lademann, A. V. Priezzhev and R. Myllylä, *J. Biomed. Opt.*, 2005, **10**, 064037.
5 J. Lademann, S. Schanzer, U. Jacobi, H. Schaefer, F. Pflücker, H. Driller, J. Beck, M. Meinke, A. Roggan and W. Sterry, *J. Biomed. Opt.*, 2005, **10**, 014008.
6 A. O. Rybaltovskii, V. N. Bagratashvili, A. I. Belogorokhov, V. V. Koltashev, V. G. Plotnichenko, A. P. Popov, A. V. Priezzhev, A. A. Sviridova, K. V. Zaĭtseva, I. A. Tutorskii and A. A. Ishchenko, *Opt. Spectrosc.*, 2006, **101**, 590–596.
7 E. S. Thiele and R. H. French, *J. Am. Ceram. Soc.*, 1998, **81**, 469–479.
8 A. Usami and H. Ozaki, *J. Phys. Chem. B*, 2005, **109**, 2591–2596.
9 L. E. McNeil, A. R. Hanuska and R. H. French, *Appl. Opt.*, 2001, **40**, 3726–3736.
10 L. E. McNeil and R. H. French, *Acta Mater.*, 2000, **48**, 4571–4576.
11 M. Cho and J. Yoon, *J. Appl. Microbiol.*, 2008, **104**, 759–766.
12 C. Chen, P. Lei, H. Ji, W. Ma, J. Zhao, H. Hidaka and N. Serpone, *Environ. Sci. Technol.*, 2004, **38**, 329–337.
13 Q. Xiao, Z. Si, J. Zhang, C. Xiao and X. Tan, *J. Hazard. Mater.*, 2008, **150**, 62–67.
14 T. Xia, M. Kovochich, J. Brant, M. Hotze, J. Sempf, T. Oberley, C. Sioutas, J. I. Yeh, M. R. Wiesner and A. E. Nel, *Nano Lett.*, 2006, **6**, 1794–1807.
15 V. Sharma, R. K. Shukla, N. Saxena, D. Parmar, M. Das and A. Dhawan, *Toxicol. Lett.*, 2009, **185**, 211–218.
16 W. Zhang, T. Yang, C. Yin, G. Li and K. Jiao, *Electrochem. Commun.*, 2009, **11**, 783–786.
17 H. L. Karlsson, J. Gustafsson, P. Cronholm and L. Möller, *Toxicol. Lett.*, 2009, **188**, 112–118.
18 P. Miralles, T. L. Church and A. T. Harris, *Environ. Sci. Technol.*, 2012, **46**, 9224–9239.
19 S. Rocheleau, M. Arbour, M. Elias, G. I. Sunahara and L. Masson, *Nanotoxicology*, 2015, **9**, 502–512.
20 T. Tong, C. M. Wilke, J. Wu, C. T. T. Binh, J. J. Kelly, J.-F. Gaillard and K. A. Gray, *Environ. Sci. Technol.*, 2015, **49**, 8113–8123.
21 J. Wang, G. Zhou, C. Chen, H. Yu, T. Wang, Y. Ma, G. Jia, Y. Gao, B. Li, J. Sun, Y. Li, F. Jiao, Y. Zhao and Z. Chai, *Toxicol. Lett.*, 2007, **168**, 176–185.
22 S. Dalai, S. Pakrashi, R. S. S. Kumar, N. Chandrasekaran and A. Mukherjee, *Toxicol. Res.*, 2012, **1**, 116–130.
23 H. Liu, L. Ma, J. Zhao, J. Liu, J. Yan, J. Ruan and F. Hong, *Biol. Trace Elem. Res.*, 2009, **129**, 170–180.
24 A. Simon-Deckers, S. Loo, M. Mayne-L'hermite, N. Herlin-Boime, N. Menguy, C. Reynaud, B. Gouget and M. Carrière, *Environ. Sci. Technol.*, 2009, **43**, 8423–8429.
25 X. Chen and S. S. Mao, *Chem. Rev.*, 2007, **107**, 2891–2959.
26 C. Y. Jin, B. S. Zhu, X. F. Wang and Q. H. Lu, *Chem. Res. Toxicol.*, 2008, **21**, 1871–1877.
27 J. Chen, H. Zhou, A. C. Santulli and S. S. Wong, *Chem. Res. Toxicol.*, 2010, **23**, 871–879.
28 Z. E. Allouni, P. J. Høl, M. A. Cauqui, N. R. Gjerdet and M. R. Cimpan, *Toxicol. In Vitro*, 2012, **26**, 469–479.
29 L. Shang, K. Nienhaus and G. U. Nienhaus, *J. Nanobiotechnol.*, 2014, **12**, 5–5.

30 K. Suttiponparnit, J. Jiang, M. Sahu, S. Suvachittanont, T. Charinpanitkul and P. Biswas, *Nanoscale Res. Lett.*, 2011, **6**, 27–27.
31 D. B. Warheit, T. R. Webb, C. M. Sayes, V. L. Colvin and K. L. Reed, *Toxicol. Sci.*, 2006, **91**, 227–236.
32 C. Jin, Y. Tang, F. G. Yang, X. L. Li, S. Xu, X. Y. Fan, Y. Y. Huang and Y. J. Yang, *Biol. Trace Elem. Res.*, 2011, **141**, 3–15.
33 S. Wang, Z. Melkoumian, K. A. Woodfork, C. Cather, A. G. Davidson, W. F. Wonderlin and J. S. Strobl, *J. Cell. Physiol.*, 1998, **176**, 456–464.
34 J. Wu, J. Sun and Y. Xue, *Toxicol. Lett.*, 2010, **199**, 269–276.
35 S. Huang, P. J. Chueh, Y. W. Lin, T. S. Shih and S. M. Chuang, *Toxicol. Appl. Pharmacol.*, 2009, **241**, 182–194.